International Journal of Engineering Sciences &Research Technology
(A Peer Reviewed Online Journal)
Impact Factor: 5.164

➕ **IJESRT**

Chief Editor
Dr. J.B. Helonde

Executive Editor
Mr. Somil Mayur Shah

IJESRT

INTERNATIONAL JOURNAL OF ENGINEERING SCIENCES & RESEARCH TECHNOLOGY
CFD ANALYSIS OF FLOWFIELD IN A GENERIC ENGINE NACELLE

Sanjay Shanmugasundaram*[1] & Peter J. Disimile[2]
*[1]MS Aerospace Engineering, University of Cincinnati, Cincinnati, OH, US
[2]Associate Professor, Department of Aerospace Engineering, University of Cincinnati, Cincinnati, OH, US

ABSTRACT

This paper deals with the study of airflow in an uncluttered nacelle, as an important first step in setting up the basis for further analysis of suppressant transport within an aircraft engine nacelle. This initial study will help establish a viable CFD model to study the nacelle air flow conditions at typical Reynolds numbers, by studying the effects of different turbulence models, boundary conditions as well as the computational grids used in the simulation. Initial boundary conditions were derived from a report by Sandia National Laboratories (SNL). Validation cases were run using different input conditions, based on either the experimental conditions or based on a user-defined function and the validity of current simulations were ascertained by comparing velocity profiles and turbulence intensity profiles at different measurement stations. Effects of the computational grids were examined by carrying out a grid sensitivity study. The sensitivity of the simulations to different turbulence models, was also studied, to see if the discrepancies in the velocity and turbulence intensity profiles, near the walls, noticed in some sections, could be resolved. The current simulations showed reasonable agreement to the experimental data and very good agreement with the CFD-ACE obtained data from the simulations performed by SNL.

KEYWORDS: Engine nacelle, air flow, CFD, RANS turbulence modelling, velocity, turbulence intensity, mesh types

1. INTRODUCTION

Fire protection in aircraft engine nacelles is extremely important as it helps save lives, allows for mission completion and reduces damage caused by flame impingement or increased thermal loads. Given the new regulations banning or restricting the use of environmentally harmful but effective fire suppressant agents like Halon 1301 etc., it has become extremely important to study and develop more optimized methods of fire suppression delivery in aircraft engine nacelles. The Next Generation Fire Suppression Technology program (NGP) was initiated by the US Department of Defense in FY 1997, to develop new fire suppressants that meet the operational requirements currently satisfied by Halon 1301and also develop improved agent delivery techniques [1]. While there are studies being conducted to develop new chemical replacements for traditional compounds like halons, these new agents also have higher boiling points and greatly reduced fire suppression effectiveness and to date, none have been considered as an acceptable replacement. This would result in the need to carry additional amounts of the agent as compared to the amounts needed with Halon, resulting in added weight and size of the fire suppression system. It is therefore equally important to come up with improved/optimized suppressant transport and dispersion systems, to account for the various factors such as efficiency in extinguishing fires, weight considerations as well as distribution effects due to the different operating conditions of the aircraft engines. Hamins et al [2], conducted a set of experiments to study the influence of various parameters affecting flame stability within an aircraft engine nacelle. These experiments indicated that fire hazards in an engine nacelle depend on a variety of parameters such as, air velocity, nacelle temperature, fuel type, and system pressure etc. Hamins et al, also developed a simple model to predict the impact of these factors on fire suppression. The model helped gain an understanding of how factors such as injection duration, air flow, nacelle free volume, fluid mixing and fire scenario etc., impact minimum agent suppression requirements, with air flow and nacelle volume being the best predicted parameters. Crawford et al, [3] conducted a series of CFD simulations to study the dispersion of fire suppressant N_2 in an idealized nacelle,

using two different injection nozzles and in some cases, the presence of clutter was also introduced. Various turbulence models were studied and in general Crawford et al, concluded that the standard k-ε and the realizable k-ε gave the best results. They also concluded that in some cases adaptive mesh refinement was needed to replicate the observed experimental data, especially in the N_2 plume region. From the studies performed by Crawford et al, [3] a general understanding of the type of turbulence models that may be used to capture transport of fire suppressants in an engine nacelle and the grid requirements needed for accurate representation of the suppressant dispersion was highlighted. J.C. Hewson et al, [4] presented suppression modelling employed in CFD codes with an emphasis on fire suppression in cluttered elements. CFD results were used to analyze the effect of geometrical changes on suppressant distribution. They presented a suppression model based on a critical Damkohler number for extinction and was suitable for use in CFD codes. They implemented this model into a Vulcan fire field model and evaluated by comparing a case of pool fire suppression in a wind tunnel behind a step. Effects of clutter and geometrical changes were also studied, presenting an idea of how fire suppressant distribution and suppression phenomenon are impacted by these factors. J.C.H ewson and D.R.Keyser [5], used the Vulcan fire-field model to simulate the evolution of pool fires and the distribution of fire suppressants in a nacelle simulator. Their primary objective was to identify conditions in which fire suppression was successful and conditions for which it was not. They predicted that as the rate of suppressant injection was reduced by a third or more, some regions of the nacelle did not receive the necessary amount of fire suppressant to achieve suppression. They also predicted that removal of certain nozzles introduced substantial in homogeneities in the suppressant distribution. Likewise, capping certain nozzles did not have an effect on the suppression capabilities while capping others caused a failure to suppress the fires, indicating the location of nozzles inthe domain had an impact on fire suppressant distribution. This made it abundantly clear that a thorough understanding of a nacelle air flow was of paramount importance if an attempt to understand the importance ofthe effect of suppressant injection location on suppressant distribution. Of all the factors that affect fire suppression, the primary airflow and turbulence level in an engine nacelle are the basic and most important parameters of all as theyhelp define the flow-field and the level of mixing with-in the nacelle. This in turn helps identify points of recirculation and stagnation zones in an engine nacelle, which tend to serve as good flame holders, making flame extinction difficult. Therefore, it is important to study the primary flow field within an engine nacelle, thereby gaining an understanding of different fire zones and ultimately guiding the design of an efficient fire suppression system.A.R Black et al [6], which are referred to as the SNL studies, conducted a series of experiments evaluating the air flow in an idealized quarter scale engine nacelle simulator. CFD simulations using CFD-ACE and VULCAN were also conducted in tandem with these experiments to see how well the models performed in relation to the experiments. They concluded that the computational models did a good job at replicating the experimental velocity and turbulence intensity profiles across different cross-sections within the nacelle. The same geometry was considered for the present study as it gave a good basis to study the effectiveness of using ANSYS Fluent to capture the flow field in an idealized engine nacelle. SNL [6] did conduct a rudimentary study to see the effect of different turbulence models, but a comprehensive comparison of various turbulence models was not presented. Hence the current study will also include a comprehensive look at different turbulence models, especially a few involving near-wall modelling, in order to see if the gap between the experimental and computational data from SNL study at certain measuring planes could be resolved. The primary objective of this study is to establish that ANSYS fluent can be used to effectively capture the flow field in an ideal engine nacelle and to highlight the best computational model (including turbulence model, computational grid, boundary conditions) needed to better replicate the experimental results from the reference study [6].

2. COMPUTATIONAL MODEL

Governing Equations and Turbulence Models
Fluid dynamics is governed by three fundamental equations, the conservation of mass, momentum and energy. These form the cornerstone upon which Computational Fluid Dynamics is based on.

The time-averaged momentum equations known as the Reynolds Averaged Navier-Stokes equations (RANS Equations) obtained using Reynolds decomposition are the basis for the current computations. Since most CFD simulations are typically interested in time-averaged properties of the flow, the RANS formulation is the primary choice.

The tensor form of the RANS equations is given by,

$$\rho \frac{D\bar{u}_i}{Dt} = F_i - \frac{\partial \bar{p}}{\partial x_i} + \mu \Delta \bar{u}_i - \rho \left(\frac{\partial \overline{u_i' u_j'}}{\partial x_j} \right) \tag{i}$$

The total shear stress term obtained from the above equation results in,

$$\tau_{ij} = \mu \frac{\partial u_i}{\partial x_j} - \rho \overline{u_i' u_j'} \tag{ii}$$

The additional term apart from the viscous term, that is present in the total shear stress expression, is termed as Reynolds stress and is a result of the time averaging of the RANS equations. The nonlinearity of the Reynolds stress term in the RANS equations, results in the need to close the RANS equations by modelling the Reynolds stress term as a function of the mean flow. This is done by removing any reference to the fluctuating part of the velocity. This is the closure problem associated with RANS equations. The concept of eddy viscosity is used to tackle the closure problem, where the Boussinesq hypothesis is applied to the Reynolds stress term and the additional turbulence stresses are given by augmenting the molecular viscosity with an eddy viscosity.

There are many different turbulence models that have been developed to account for the Reynolds stresses in the RANS equations. Using different transport properties there are many algebraic models, one equation models, two-equation models etc. Based on how eddy viscosity is modelled there are Linear and non-linear eddy viscosity models. An overview of these models is presented in the next sections.

Turbulence models
The primary turbulence models considered for this study were the two equation Linear eddy viscosity models, Standard k-ε model, Realizable k-ε model, Wilcox's k-ω model and SST k-ω model. The standard k-ε model used in this study employed both the standard wall functions and enhanced wall functions, while the Realizable k-ε model used in this study employed only the enhanced wall functions. The enhanced wall functions were employed to study the near wall properties as detailed later.

Standard k-ε model – This is the most commonly used model in CFD. It is a two-equation model, that uses two transport equations to give a general description of turbulence by modeling the turbulence kinetic energy (k) and the rate of dissipation of turbulence energy (ε).

The transport equations for the standard k-ε model are,
For turbulent kinetic energy k,

$$\frac{\partial}{\partial t}(\rho k) + \frac{\partial}{\partial x_i}(\rho k u_i) = \frac{\partial}{\partial x_j}\left[\left(\mu + \frac{\mu_t}{\sigma_k}\right)\frac{\partial k}{\partial x_j}\right] + P_k + P_b - \rho \epsilon - Y_M + S_k \tag{iii}$$

For dissipation ε,

$$\frac{\partial}{\partial t}(\rho \varepsilon) + \frac{\partial}{\partial x_i}(\rho \varepsilon u_i) = \frac{\partial}{\partial x_j}\left[\left(\mu + \frac{\mu_t}{\sigma_\varepsilon}\right)\frac{\partial \varepsilon}{\partial x_j}\right] + C_{1\varepsilon}\frac{\varepsilon}{k}(P_k + C_{3\varepsilon}P_b) - C_{2\varepsilon}\rho\frac{\varepsilon^2}{k} + S_\varepsilon \tag{iv}$$

Turbulent viscosity, μ_t is modelled as,

$$\mu_t = \rho C_\mu \frac{k^2}{\varepsilon} \tag{v}$$

Realizable K-ε model – This model was developed with some variations made to the transport equations of the standard k-ε model. It provides a better prediction of jet spread rates and is in general better at capturing the mean flow of complex flow structures.

The transport equations for the Realizable k-ε model are,
For the turbulent kinetic energy k,

$$\frac{\partial}{\partial t}(\rho k) + \frac{\partial}{\partial x_j}(\rho k u_j) = \frac{\partial}{\partial x_j}\left[\left(\mu + \frac{\mu_t}{\sigma_k}\right)\frac{\partial k}{\partial x_j}\right] + P_k + P_b - \rho \epsilon - Y_M + S_k \tag{vi}$$

For dissipation ε,

$$\frac{\partial}{\partial t}(\rho \varepsilon) + \frac{\partial}{\partial x_j}(\rho \varepsilon u_j) = \frac{\partial}{\partial x_j}\left[\left(\mu + \frac{\mu_t}{\sigma_\varepsilon}\right)\frac{\partial \varepsilon}{\partial x_j}\right] + \rho C_1 S_\varepsilon - \rho C_2 \frac{\varepsilon^2}{k + \sqrt{v\varepsilon}} + C_{1\varepsilon}\frac{\varepsilon}{k}C_{3\varepsilon}P_b + S_\varepsilon \tag{vii}$$

The turbulence viscosity, μ_t is modelled in the same way as standard k-ε, with some difference made in the calculations of the constant,

$$\mu_t = \rho C_\mu \frac{k^2}{\varepsilon}$$
(viii)

K-ω model–It is another two-equation model, that is used as a closure for the RANS equation. It does this by using two transport equations to solve for turbulence kinetic energy (k) and specific rate of dissipation (ω). This model is primarily used for wall bounded flows where wall effects are felt.

The transport equations for the k-ω turbulence model are,

For the turbulent Kinetic energy k,

$$\frac{\partial k}{\partial t} + U_j \frac{\partial k}{\partial x_j} = \tau_{ij} \frac{\partial U_i}{\partial x_j} - \beta^* k\omega + \frac{\partial}{\partial x_j}\left[(\nu + \sigma^* \nu_T)\frac{\partial k}{\partial x_j}\right]$$
(ix)

For the specific dissipation rate ω,

$$\frac{\partial \omega}{\partial t} + U_j \frac{\partial \omega}{\partial x_j} = \alpha \frac{\omega}{k} \tau_{ij} \frac{\partial U_i}{\partial x_j} - \beta \omega^2 + \frac{\partial}{\partial x_j}\left[(\nu + \sigma \nu_T)\frac{\partial \omega}{\partial x_j}\right]$$
(x)

The kinematic eddy viscosity, ν_T is given by,

$$\nu_T = \frac{k}{\omega}$$
(xi)

SST K-ω model– The SST k-ω model is a robust two-equation eddy viscosity model used to tackle the closure problem of RANS equations. This model combines the k-ε model with the k-ω model in a way that it uses k-ω in the inner parts of the boundary layer and switches to k-ε in the free-stream. This way, the model can be used to capture the flow through the viscous sub-layer down to the wall and at the same time avoid the k-ω model's problem of strong freestream sensitivity. This model again uses two transport equations to solve for the turbulence kinetic energy (k) and the specific dissipation rate (ω).

The transport equations, employed by this model are,

For the turbulence kinetic energy k,

$$\frac{\partial k}{\partial t} + U_j \frac{\partial k}{\partial x_j} = min\left(\tau_{ij}\frac{\partial U_i}{\partial x_j}, 10\beta^* k\omega\right) - \beta^* k\omega + \frac{\partial}{\partial x_j}\left[(\nu + \sigma_k \nu_T)\frac{\partial k}{\partial x_j}\right]$$
(xii)

For the specific dissipation rate ω,

$$\frac{\partial \omega}{\partial t} + U_j \frac{\partial \omega}{\partial x_j} = \alpha S^2 - \beta \omega^2 + \frac{\partial}{\partial x_j}\left[(\nu + \sigma_\omega \nu_T)\frac{\partial \omega}{\partial x_j}\right] + 2(1-F_1)\sigma_{\omega^2}\frac{1}{\omega}\frac{\partial k}{\partial x_i}\frac{\partial \omega}{\partial x_i}$$
(xiii)

Where F_1 is given by,

$$F_1 = tanh\left\{\left\{min\left[max\left(\frac{\sqrt{k}}{\beta^*\omega y}, \frac{500\nu}{y^2\omega}\right), \frac{4\sigma_{\omega^2}k}{\left(max\left(2\rho\sigma_{\omega^2}\frac{1}{\omega}\frac{\partial k}{\partial x_i}\frac{\partial \omega}{\partial x_i}, 10^{-10}\right)\right)y^2}\right]\right\}^4\right\}$$
(xiv)

The kinematic eddy viscosity is given by,

$$\nu_T = \frac{\alpha_1 k}{max\left(\alpha_1\omega, Stanh\left[\left[max\left(\frac{2\sqrt{k}}{\beta^*\omega y}, \frac{500\nu}{y^2\omega}\right)\right]^2\right]\right)}$$
(xv)

Geometry setup

There are two basic geometries considered for simulations in the current study. The first is a long inlet geometry that models the experimental setup that was used in the reference study [6]. This geometry captures all the details downstream from the inlet flow conditioners up to approximately 10 diameters downstream from the trailing edge of the simulated engine core. The second geometrical model is a short inlet geometry modelled again off the same experimental setup, but this time from a location referred to as MS-1 (see Table 1 for details), just upstream from the engine core and extending 10 diameters downstream past the trailing edge of the engine core. The two geometries are used to understand and study different approaches that are being considered for validating our computational model with minimal computational resources. Figure 1 describes the general geometric configurations.

long inlet geometry – The long inlet geometry is used as a basis for a computational approach based on the boundary conditions being derived from the experimental conditions from the reference study [6]. This approach allows for computational replication of experimental conditions and provides a check on the differences between the different approaches used in the current study. A generic quarter scale engine flow facility was used in the experiments.

Short inlet geometry – To enable the use of a user-defined function to describe the turbulent velocity and turbulent intensity at MS-1, the short inlet geometry is used, with MS-1 designated as the inlet. This enables us to replicate the methodology followed by SNL in their computational analysis. To validate the current computations, the resultswere compared with the CFD simulations done by SNL using VULCAN and CFD ACE [6]. Inlet profiles from an 8m long pipe were also used to run simulations on the short inlet geometry, to eliminate the dependence on experimental data at station MS-1. This methodology provided a way to save on computational resources when more practicalgeometries are examined, like an operational engine nacelle. For example, analysis involving the addition of clutter elements, introduction of secondary or injection flow (introducing a fire suppressant) etc., would only need the short inlet geometry (nacelle region) to be simulated and the long inlet upstream profiles can be obtained from an initial computation from a long pipe or by using a user defined function.

Details of both the geometries used in the computations are described in Table 1.

Table 1. Details of the long inlet and short inlet geometries

| GEOMETRY DETAILS / MEASUREMENT LOCATIONS		LOCATIONS W.R.T INLET	
STATION	DESCRIPTION OF LOCATION	mm	mm
reference 1	flow conditioner exit [1] - **Flow inlet for long inlet geometry**	0	-
MS-1	Upstream from Inlet cone (core) LE - **Flow inlet for short Inlet geometry**	6213.475	0
reference 2	Start of Inlet Transition Duct (ITD)	6831.584	618.109
reference 3	Inlet cone LE (Engine core)	6832.6	619.125
MS-3	Downstream of Inlet cone (core) LE but within ITD	6892.925	679.45
MS-5	Downstream of Inlet cone (core) LE but within ITD	7146.925	933.45
reference 4	End of Inlet Transition Duct (ITD)	7247.636	1034.161
reference 5	Inlet Cone TE (Engine core)	7261.352	1047.877
MS-7	Downstream of ITD (Upstream of ETD)	7861.3	1647.825
reference 6	Start of Exit Transition Duct (ETD)	8466.836	2253.361
reference 7	Exit cone LE (Engine core)	8466.836	2253.361
MS-9	Downstream of Exit cone (core) LE but within ETD	8663.686	2450.211
reference 8	End of Exit Transition Duct (ETD)	8882.888	2669.413
reference 9	Exit cone TE (Engine core)	8898.636	2685.161
MS-11	Downstream of Exit cone (core) TE	9508.236	3294.761
reference-10	Flow Exit (10 diameters from Exit cone (core) TE)	10422.636	4209.161
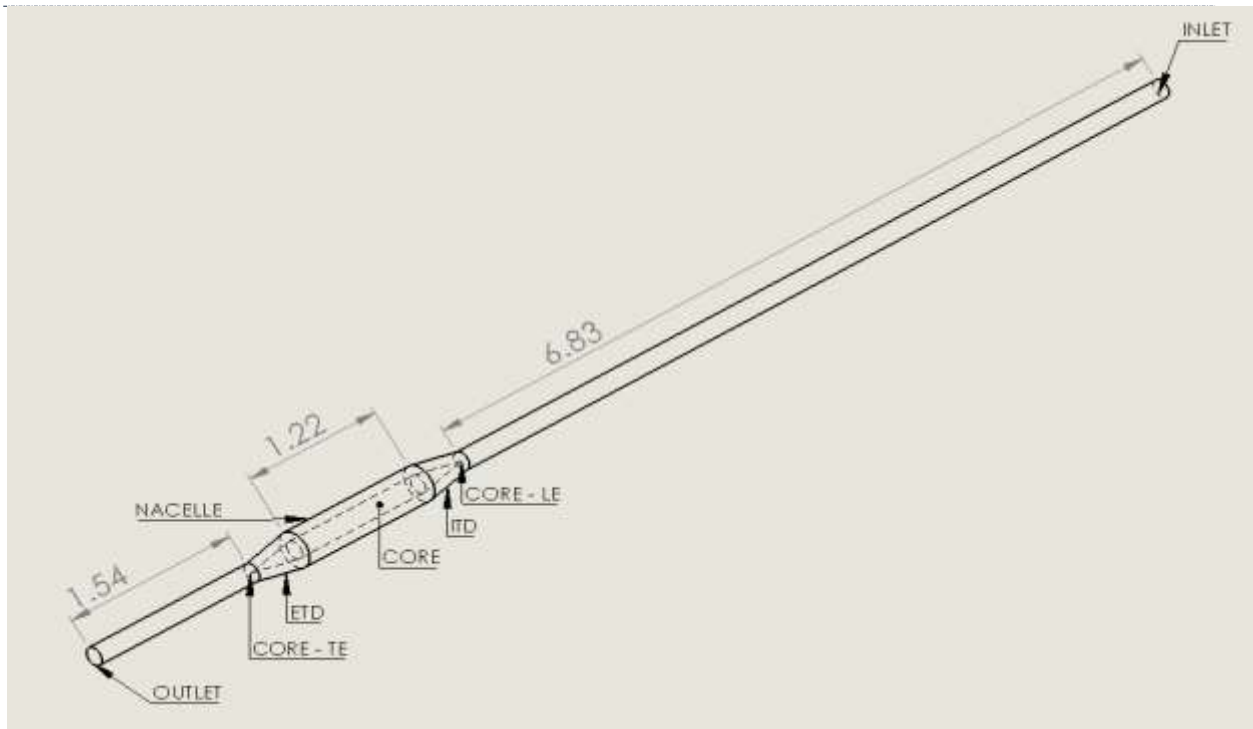
Figure 1. Details of the long inlet geometry

Meshing –
ANSYS ICEM was utilized to create all the meshes (unstructured and structured) used in the current study. Both the structured and unstructured meshes were examined and reported in the next section.

Unstructured mesh –
The initial validation cases employed a standard k-ε model with standard wall functions, which requires a mesh with a wall Y+ of *at least* 30. Also considering the geometry, a solid inner core region with conical ends, it was not advisable to generate a structured mesh using hexahedral elements, as the conical ends of the geometry would cause the mesh to be highly skewed towards the conical tips which would result in poor accuracy. The conical tips also result in singular grid topologies (axis points). These should be avoided as they tend to make a structured mesh have highly skewed/small elements in such regions which are detrimental to flow-solver stability and to the accuracy of the computations. In order to avoid these issues, an unstructured tetrahedral mesh was utilized. Unstructured meshes were used for both the long inlet and the short inlet geometries, where the core was not modified. A combination of Octree and Delaunay meshes were used to perform a grid sensitivity test while validating the current computations against the experimental and CFD results reported by SNL [6]. To comply with the turbulence model being used, the meshes were created in such a way that a wall Y+ of at least 30 was always maintained. The Octree method starts by generating a volume mesh using a top-down approach which is made to conform with the geometry, after which, patch independent surface meshes are created at all the boundaries and inner walls. Delaunay Mesh generation is done in two steps, the first being placement of Steiner points and the second being Delaunay triangulation. One common method to generate a Delaunay mesh is to use the robust Octree approach to generate a surface mesh and then generate a volume mesh using the Delaunay method. A multitude of Octree and Delaunay meshes were used to perform a grid sensitivity study, and it was found that the Delaunay meshes were preferred, due to the Delaunay method resulting in a more uniform mesh than an Octree method thereby helping us avoid regions of coarse meshing.

Structured mesh –
A structured mesh was desired in order to carry out tests using different turbulence models, with a focus on getting improved resolution near the wall. The various turbulence models used for this purpose required meshes with a wall Y+ of less than 1. To achieve this using an unstructured mesh would result in the use of prism layers

which either results in a highly refined mesh with a reasonable growth rate between successive elements or a mesh with a highly irregular/disproportionate growth rate. This conundrum can be easily avoided by using a hexahedral structured mesh which gives us a better control over how the mesh is built. To overcome the problem of singularity at the LE and TE of the core cones, a 1mm chamfer was created at the ends of the core. This enables the use of a structured mesh with a highly refined region at the walls (maintaining wall Y = 1), while ensuring that the growth rate between successive mesh elements is maintained at 1.3.

Boundary conditions –

There were three different approaches considered for running the simulations in the current study. Two of these methods were based on replicating the experimental conditions while the other was based on creating a user defined function to describe the mean velocity profile as well as the turbulence intensity profile at station MS-1 (see Table 1) similar to what was done in the computational study reported by SNL [6].

The first method used the long inlet geometry, applying a velocity inlet boundary condition at the inlet assuming a uniform turbulence intensity of 10%. The velocity inlet conditions were based on the experimental conditions, with Reynolds number (Re) being the primary value of concern. Since there were some slight inconsistencies in the reported values by SNL, such as Re, mass flow rate and inlet velocity based on the corresponding viscosity ratio, the inlet parameters were computed with the Re being fixed at 172,000 and back calculating the inlet velocity for standard temperature and pressure. The inlet conditions used is described in table 2.

Table 2. Inlet conditions

V_{inlet}	16.945 m/s
Re	172,000
T	293 K
P	101,325 Pa
μ	1.20696 kg/m^3
ρ	1.81212e-5 kg/ m s

The second method applied, utilized a user defined function (UDF) to replicate the experimental velocity and turbulence intensity profiles at MS-1. This was used as the inlet profile for the short inlet geometry and follows the same approach as that of SNL's computational runs, allowing a reduced computational time. Since ANSYS FLUENT does not provide a direct method to input a turbulence intensity profile, so the corresponding turbulence kinetic energy profile was utilized.

The UDF models a turbulence velocity profile using the relation,

$$\frac{u}{u_{max}} = \left(\frac{y}{R}\right)^{0.12}$$
(xvi)

where y – distance from the center, R – radius of the inlet, u – average local velocity, u_{max} – maximum local velocity value at inlet

The turbulence intensity profile that is used follows the profile described by,

$$TI(\%) = 1291.8Y^2 - 196.88Y + 13.175,$$
(xvii)

where TI – turbulence intensity and Y – distance along the diameter [0, D]. The TI profile is based on a curve fit of the observed experimental data and is related to the distance along the diameter. That is Y in the above profile ranges from one end of the diameter to the other.

The third method uses the same inlet conditions as the first (derived from the experimental conditions), on an 8m long pipe (pipe diameter the same as the inlet diameter of the long inlet geometry) with a pressure outlet boundary condition. This was used to obtain a fully developed mean velocity profile, which was used as an inlet profile for the short inlet nacelle geometry. This was done because, the concept of the UDF used by SNL [6], assumed a fully developed profile but had to depend on the experimental values to model the turbulence intensity profile. In order to avoid the dependence on the experimental values,a pipe flow was computed to produce an inlet profile for a short inlet geometry, providing the ability to easily reproduce multiple flow conditions (different Reynolds numbers) while at the same time reducing computational costs.

Further by using the turbulence profile obtained with the8m pipe as an inlet profile for a short inlet geometry, different geometrical modifications (i.e., the addition of clutter) as well as the incorporation of fire suppressant injection (different chemicals, positions, flow rates etc.) can be easily handled.

All the simulations used a pressure outlet boundary conditions and a stationary wall boundary condition at the walls.

3. RESULTS AND CONCLUSION

Validation
Based on the inlet boundary condition selected, there are three approaches that are considered for the computations conducted in this paper, as detailed earlier. For validation purposes, the current computational results were compared to the published experimental data [6]. Comparison with CFD-ACE and VULCAN data, provides an insight into the differences between the various CFD software, for the current problem application. The velocity profiles and turbulence intensity profiles at 6 different measurement stations are compared in order to validate the current computational model. The numbering of the measurement stations used follows that of the reference study [6] in order to maintain consistency when comparing the results. The different stations considered are detailed in Table 1.

Since turbulence intensity is not a direct variable used in the software for the turbulence models chosen, certain approximations were incorporated into the inlet boundary conditions. In the experiment, the turbulence Intensity (TI) is determined from the measurements using the equation,

$$TI = \frac{\sqrt{\overline{u'^2}}}{\overline{u}}$$
(xviii)

In the k-ε turbulence model, the turbulent kinetic energy is defined as,

$$k = \frac{\overline{u'^2} + \overline{v'^2} + \overline{w'^2}}{2}$$
(xix)

Since v' and w' are not accurately measured in the experiment, two different strategies were used to relateu' to k. These strategies are presented below
Approach 1: assume all cross-stream velocity functions were zero, i.e. $v' = w' = 0$.
Approach 2: assume isotropic turbulent flow, i.e., $v' = w' = u'$.

Both the VULCAN and the CFD-ACE calculations used the first approach to define the turbulent kinetic energy at the inlet plane and to solve for the turbulence intensity from the turbulence kinetic energy calculated at each measurement plane. Experimental observations conjuncture that the cross-stream velocity fluctuations were very small based on cross-stream laser doppler anemometry measurements [6].

Station –MS-1
The computational data from the three different approaches are compared to the experimental data along with the numerical boundary condition used by SNL for their computations in figure 2. The current computational mean velocity and turbulent intensity data matches the numerical boundary condition used by SNL and with the

experimental data except for the slight asymmetry in the velocity profile of the experimental data. This provided high confidence in the three approaches considered in the current study.
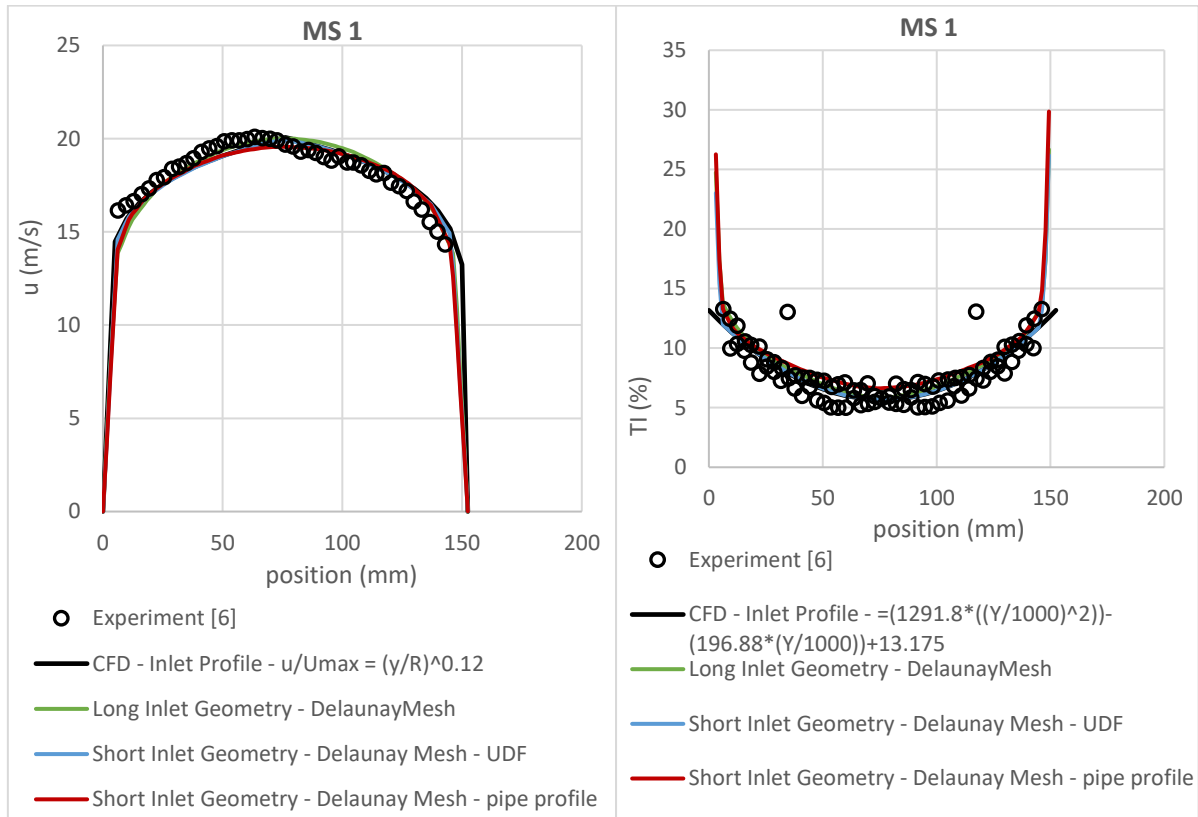

Figure 2. MS-1 – velocity profile& Turbulence Intensity profile

Station– MS-3

Station MS-3 refers to the measurement plane at the beginning of the transition region of the core (transition from inlet pipe to the annular region – ITD). Here the flow is transitioning from a developed turbulent pipe flow to a flow passing through a divergent annular channel. The data at station MS-3 is represented in figure 3. The current simulations, involving long inlet geometry and the short inlet geometry (using a profile from 8m pipe) show good agreement with the experimental velocity profile and the turbulent intensity profiles, while having an almost one to one match with the CFD-ACE data, except near the walls. The short inlet geometry simulation that employs the UDF over predicts the velocity values and therefore correspondingly underpredicts the turbulent intensity data. Similar to the SNL computations, the current simulations failed to pick up on the dip in the experimental velocity data (and corresponding jump in the turbulence intensity data) near the engine core walls.
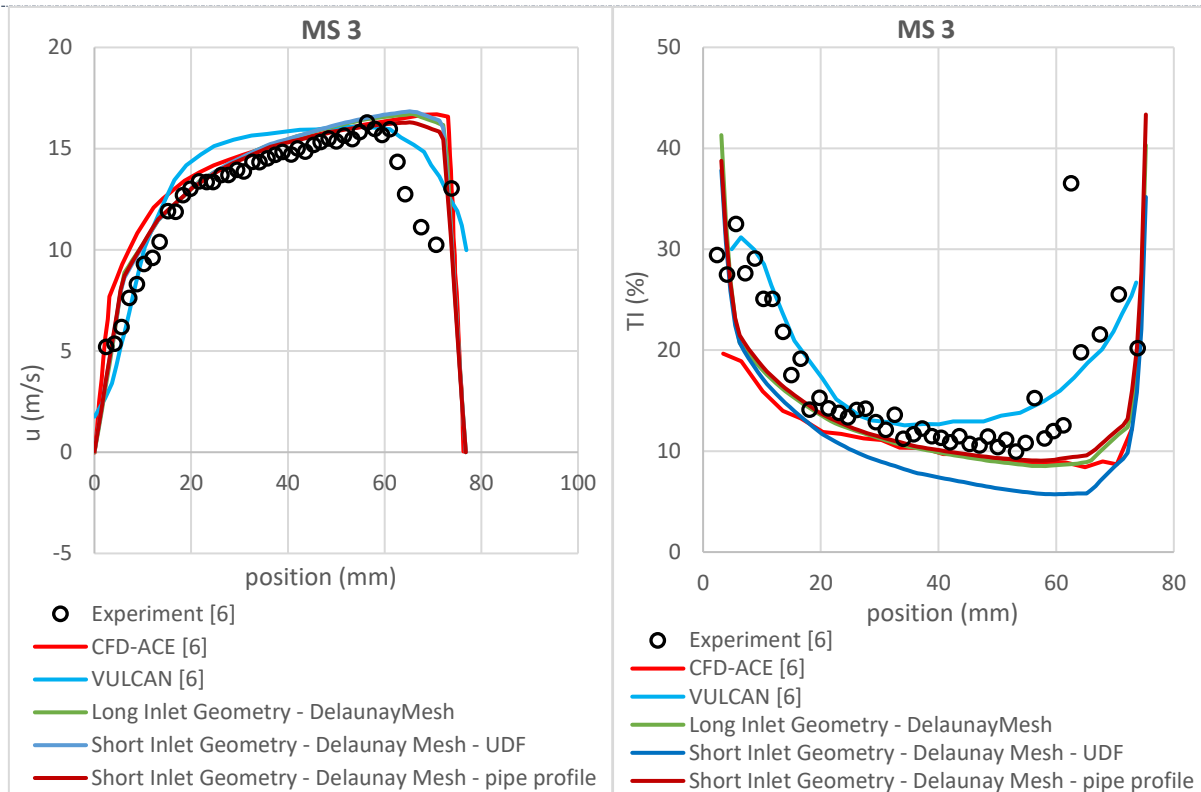
Figure 3. MS-3 – velocity profile and Turbulence intensity profile

Station– MS-5

Station MS-5 is the measurement station found just upstream of the transition zone (ITD) exit, just before the flow enters the straight, constant height annular region and the data from this station is presented in figure 4. All the current simulations show a good qualitative match with the experimental mean velocity data while having a very good quantitative and qualitative comparison with CFD-ACE data. The VULCAN data presented by SNL varies widely from both the experimental data as well as the results of the current computations. SNL attributed the narrow band of high velocity showed by VULCAN to be due to the cartesian grid that was used which caused low velocity predictions at the walls. There is a quantitative difference between the current simulation mean velocity data and the experimental data near the walls, which matches the observations made by SNL during their CFD-ACE computations. When comparing the turbulence intensity data, the current simulations showed very high TI values near the nacelle wall with a decreasing trend across the channel, again following the trend showed by CFD-ACE, having an almost exact match with the CFD-ACE data. These large differences in TI is partly due to the difference noted in the mean velocity data. The sudden jump in VULCAN TI data near the core, that is absent in the other models, was attributed by SNL to the low velocities due to the cartesian grid.
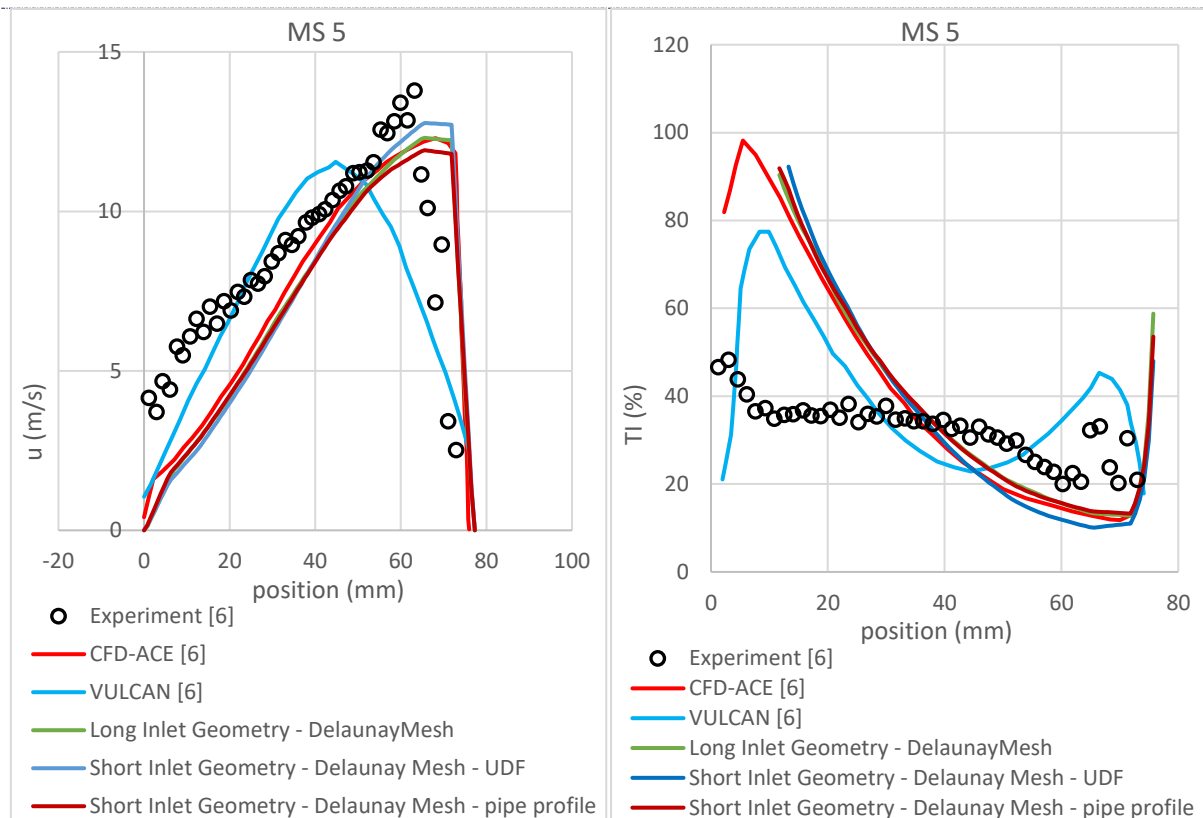
Figure 4. MS-5 – Velocity profile and Turbulence intensity profile

Station 4 – MS-7

Station MS-7 refers to the measurement plane at the mid-point of the annular region. This is the primary area of focus, since this is the fire zones of interest, location of added clutter elements as well as possible fire suppressant injector locations, etc., will be in the annular region. In Figure 5, the mean velocity predictions by the current computations showed very good agreement with the experimental data and an excellent comparison with the CFD-ACE data. The TI predictions are also within reasonable agreement with the simulation employing the UDF showing the best comparison with the experimental data, while the other two methods are a perfect match with the CFD-ACE data. VULCAN showed the poorest performance of all the models. It was observed in the reference study [6] that the experimental results don't span the entire length of the channel, all the way to the core wall and that is why both the mean velocity and TI profiles from the experiment end well before the core wall region. The current simulations replicate the high TI values found near the wall regions to a reasonable extent.
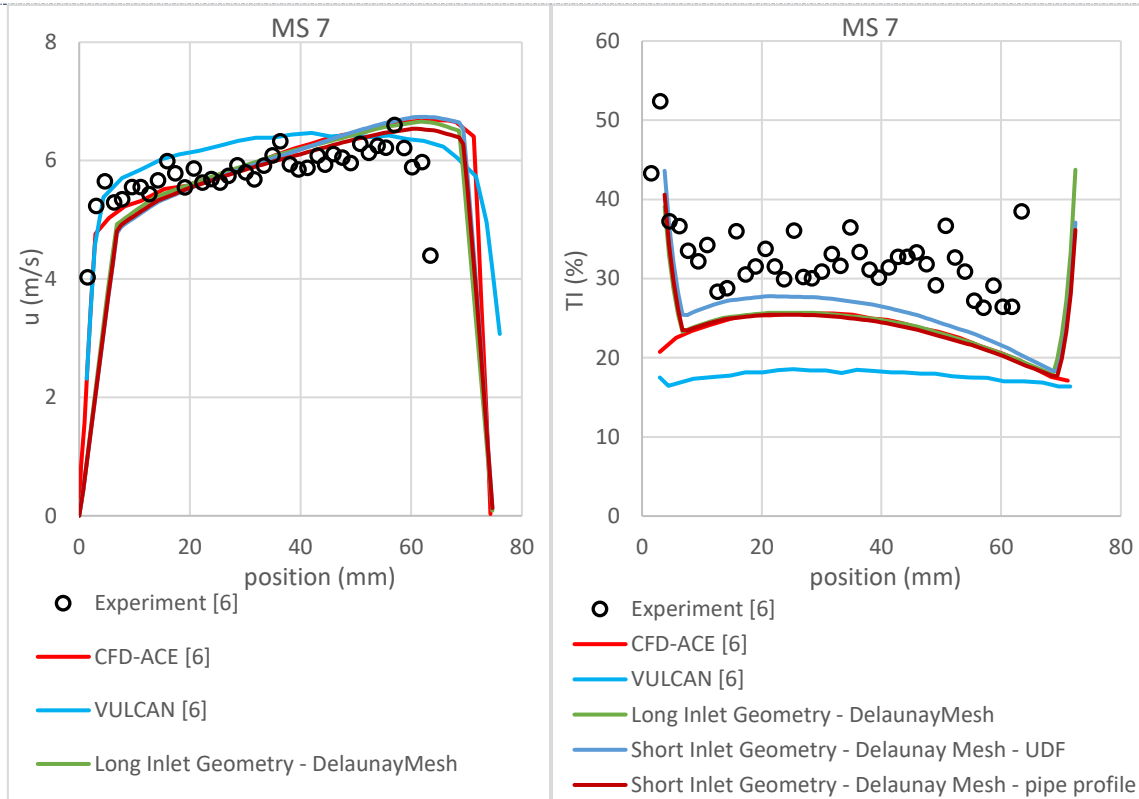
Figure 5. MS 7 – Velocity profile and Turbulence intensity profile

Station 5 – MS-9
Station MS-9 refers to the measurement station at the middle of the exit transition duct. The velocity profiles from all the current simulations show a very good agreement with both the experimental data as well as the CFD-ACE data. VULCAN results had a narrow band of high velocity which was again attributed to the stair-stepped grid [6]. When comparing the turbulence intensity profile, the current simulations, followed the same trend as the computations done by SNL, where they predicted a turbulence intensity of approximately 10% lower than that of experimental values.
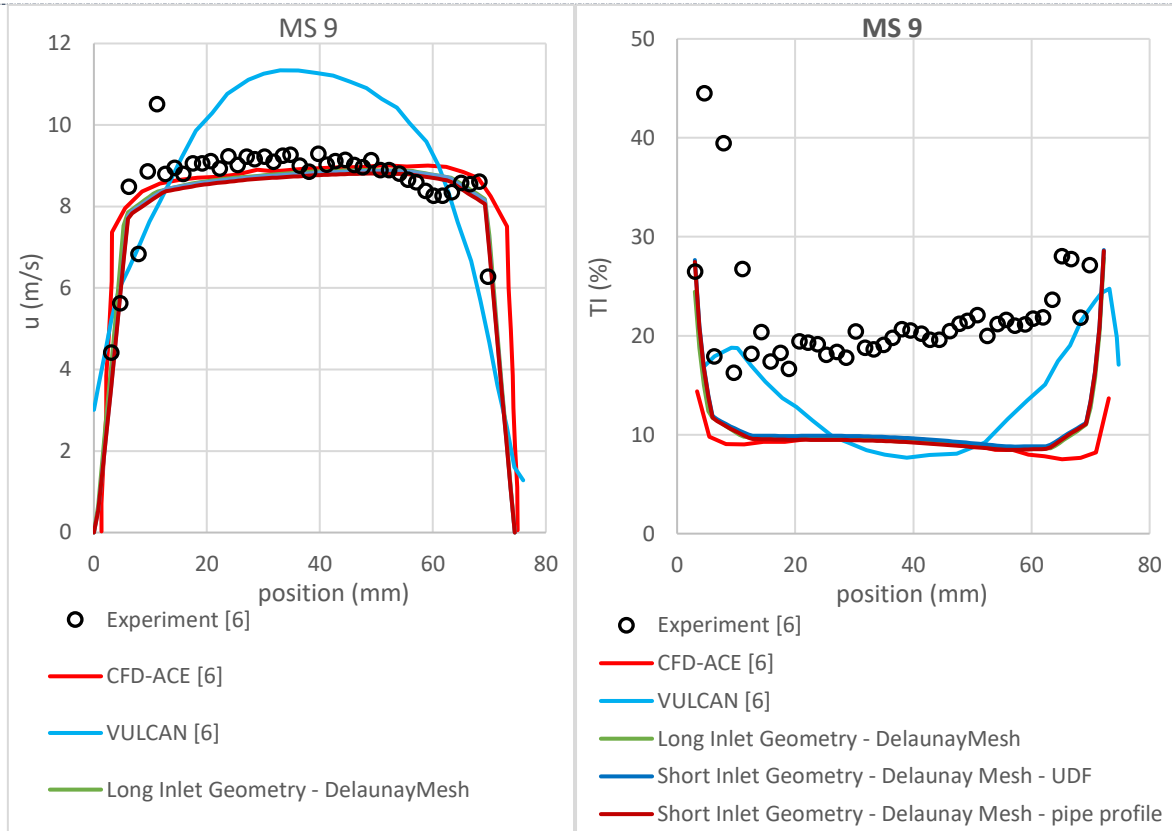
Figure 6.MS-9 – Velocity profile and Turbulence intensity profile

Station 6 – MS-11

Station MS-11 is at the exit pipe, downstream of the TE of the core region. From Figure 7, it was observed that the velocity profiles of the current simulations showed a good comparison with the experimental data as well as the computations by SNL. But unlike the CFD-ACE as well as the VULCAN simulations, the current simulations do not show a strong wake profile. The TI profiles predicted by the current simulations are in line with that predicted by CFD-ACE and very close to that of VULCAN, but just like the computations by SNL, the TI predictions by the current simulations are considerably lower than that of the experimental data. The high values of TI in the experiments, may be attributed to the noise in the velocity measurements.
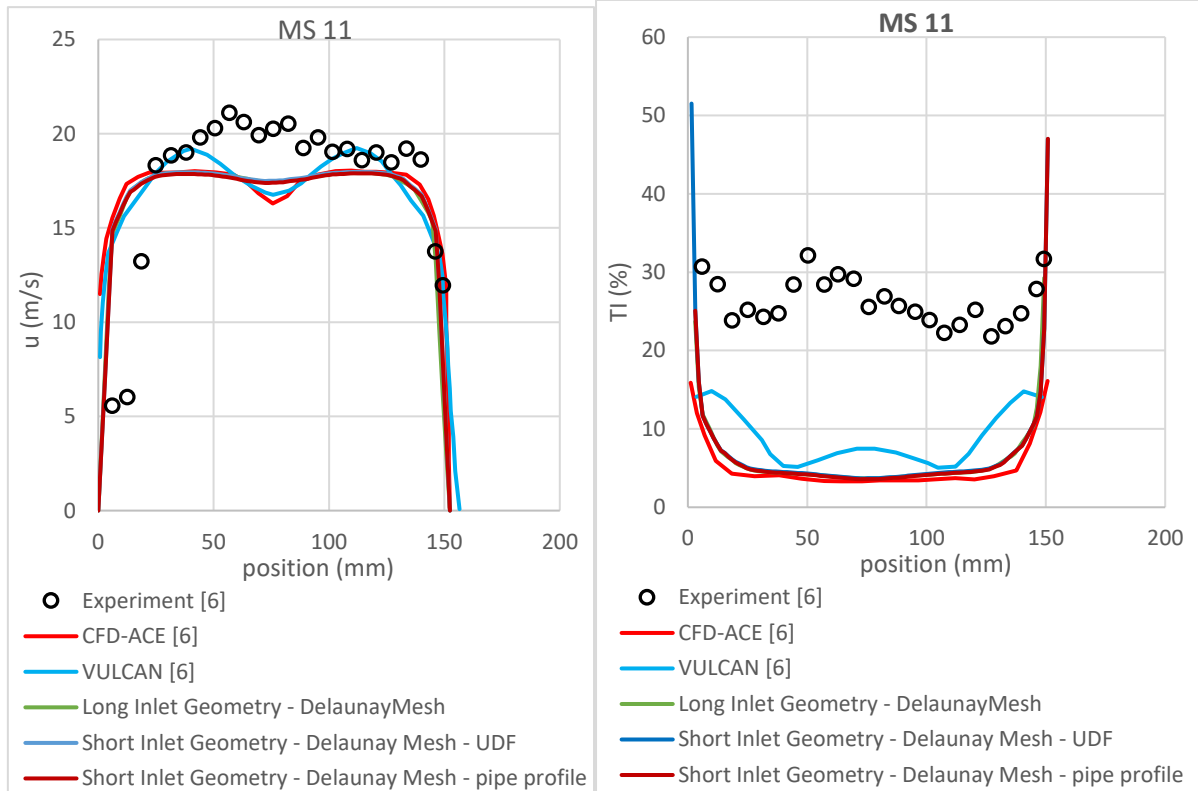
Figure 7. MS 11 – Velocity profile and Turbulence intensity profile

Also from the above comparisons, it was noted that all the three methodologies adopted for the current computations, showed very good comparison with one another thereby leading us to the conclusion that any of the three approaches could be used interchangeably based on the computational need or restrictions based of time costs and computational costs.

Root mean square value of u'

Since there was a lot of discrepancy noted near the walls in the mean velocity values in stations MS-3 and MS-5, this could have been reflected in the turbulence intensity comparisons, since the turbulence intensity is basically the root mean squared (RMS) value of the fluctuating component of velocity normalized against the mean component of the velocity.

$$TI = \frac{\sqrt{\overline{u'^2}}}{\overline{u}}$$

(xx)

Therefore, a comparison of the RMS value of the fluctuating component of the velocity was made to see if that presents a better picture of the comparison of the turbulence values.
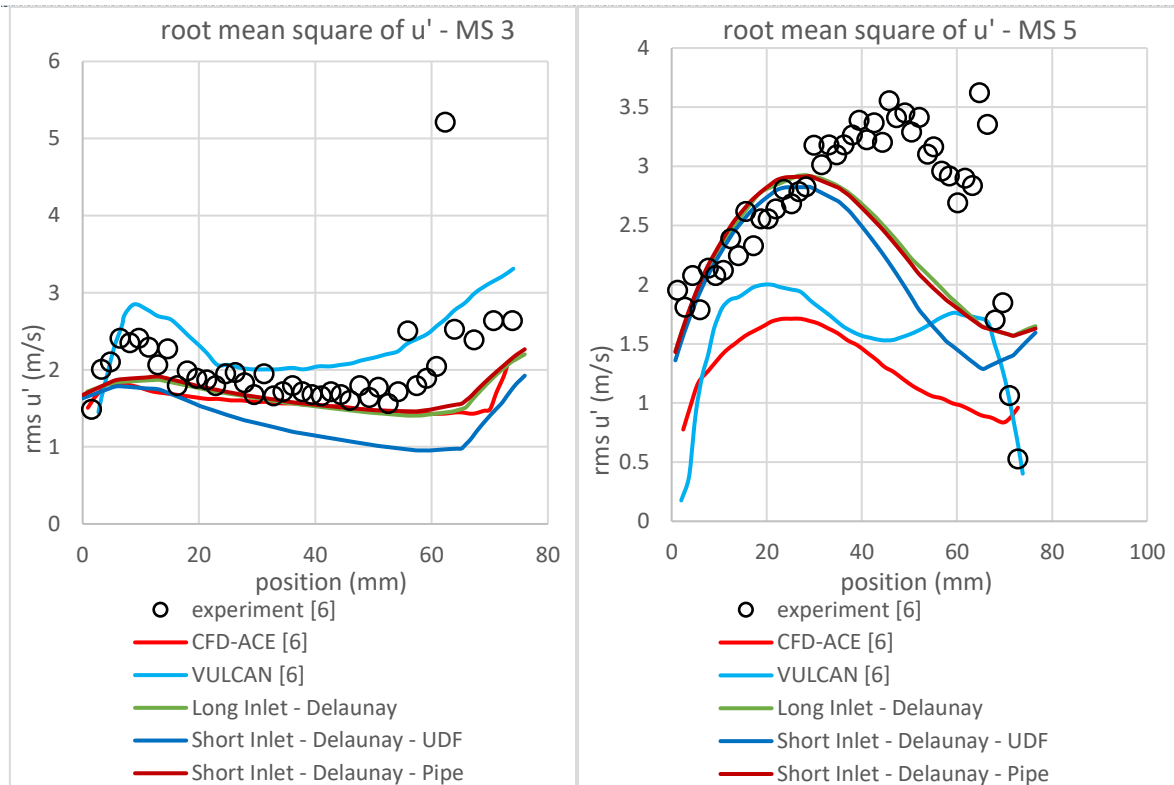
Figure 8. comparison of rms u' at measurement stations MS 3 and MS 5

At station MS – 3, it was observed that the computation based on the UDF under predicted the values when compared to the other two methods as well as both CFD-ACE and VULCAN. The long inlet geometry as well as the short inlet geometry case based on the inlet profile from an 8m pipe performed very similar to the CFD-ACE simulations, and all three showed good comparison with the experimental data. VULCAN had the best comparison with the experimental data.

At station MS – 5, it was observed that all three methods have very poor comparison near the core walls, though all three performed much better than CFD-ACE and VULCAN when compared to the experimental data [6]. All the models were in good agreement at the outer wall and fail nearer the core wall. The computations based on the UDF, slightly under predicted the values when compared to the other two methods employed in the current computations.

Grid sensitivity

In order to ensure that the current simulations were to a reasonable extent independent of the computational grid that was used, a grid sensitivity test was conducted for both the long inlet as well as the short inlet geometries. For this test, we primarily considered only the Delaunay meshes as octree meshes of larger mesh sizes were needed in order to get similar results to that of the Delaunay meshes. There was also a tendency to under predict the velocity and thereby the TI profiles when using an octree mesh.

The mean velocity and the TI values at the mid-point of station MS7 were chosen to be the parameters upon which the grid sensitivity tests were conducted. This location was chosen since it was in the middle of the channel in the center of the annular region, which represents the area of interest for all future simulations. For the long inlet geometry, a Delaunay mesh of 3.67 million elements was used for validation and for the short inlet geometry a Delaunay mesh of 2 million elements was used during validation. Grids varying from 1.97 million and up to 5 million elements were used to perform the grid sensitivity for the long inlet geometry and grids varying from 0.646 million elements to 2 million elements were used for the grid sensitivity tests for the short inlet geometry. A point to note is that the 5 million element mesh for the long inlet geometry was an octree mesh.
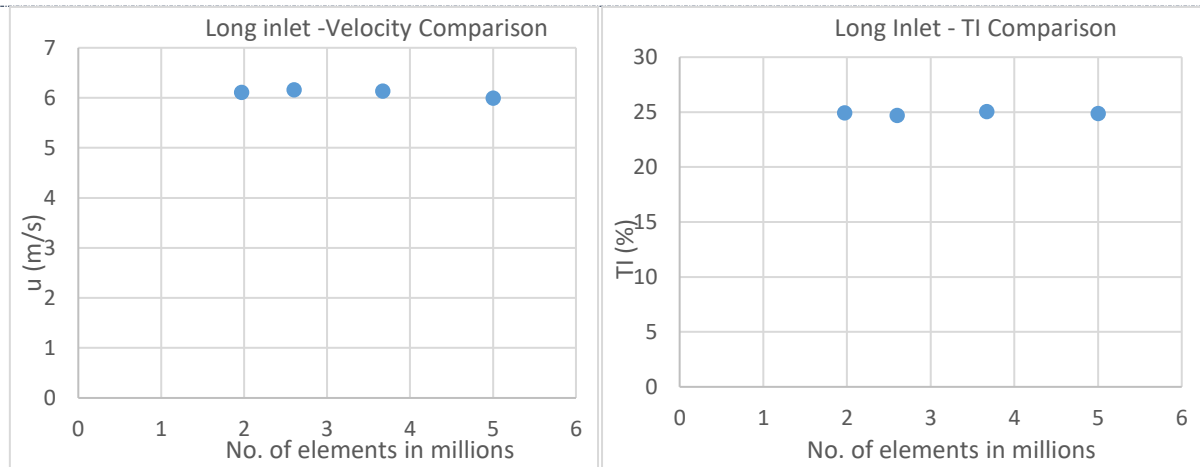
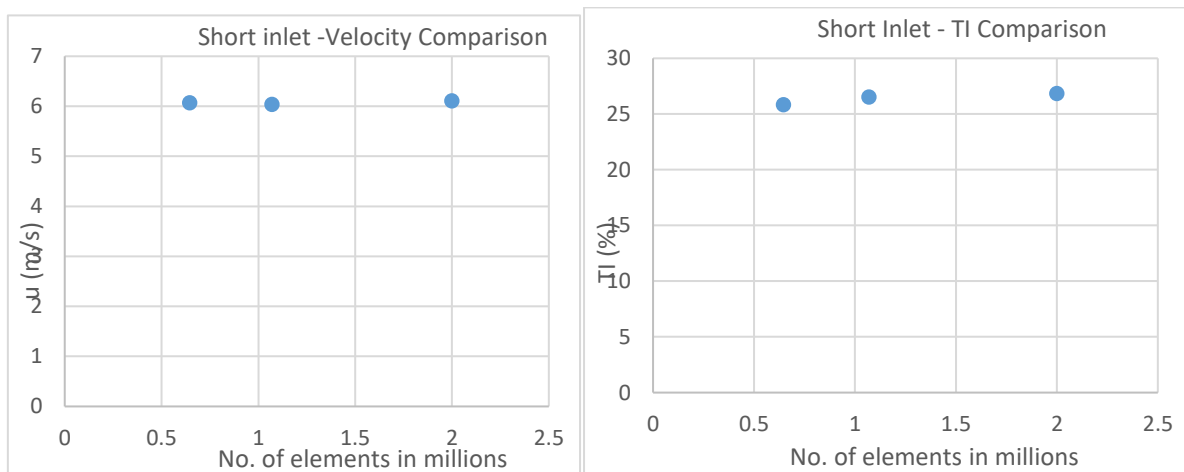*Figure 9. Grid sensitivity for long inlet geometry*

Figure 10. Grid sensitivity for short inlet geometry

From the above two sets of charts it can be observed that all the simulations considered were independent of the grid used. There was a maximum difference of 0.89% between the different grids used for the long inlet geometry, in terms of the velocity values and a maximum difference of 1.32% in terms of the TI values. When comparing the grids for the short inlet geometry, a maximum difference of 1.1% was noted in terms of the velocity values and a maximum difference of 3.89% was noted in terms of the TI values. Therefore, a Delaunay mesh of 2.6 million elements for the long inlet geometry and a Delaunay mesh of 1.07 million elements for the short inlet geometry are chosen.

Turbulence model sensitivity
As noted by the reference study [6], there were certain regions where the current simulations and even that of those performed by SNL were not able to replicate the experimental results. For example, the velocity values near the core at station MS-3, the TI values near the nacelle wall at station MS-5. It was noted that most of the differences between the experimental values and the computationally predicted values were towards the wall regions indicating that the differences might be an effect of the wall functions used and that it may be resolved by using a different turbulence model to better capture the flow properties at the walls. Therefore, it was decided that turbulence models that focused on near wall modelling would be used to see if there was any difference from the standard k-ε model employing the standard wall functions. The models chosen were std k-ε with enhanced wall functions, std k-ω, SST k-ω and realizable k-ε with enhanced wall functions. All of these used a structured mesh (involving a short inlet geometry with chamfered LE and TE on the core) and an inlet profile from an 8m pipe.

Station– MS-1

From the Figure 11, it can be observed that std k-ω and SST k-ω over predicted the velocity profile when compared with the other turbulence models. They both also showed a dip in the TI profile towards the center whereas the other turbulence models showed a smooth curve. But overall, all the turbulence models used showed a good comparison with one another with std k-ω having the largest deviation. This could be due to the std k-ω model being too sensitive to the inlet free stream properties.
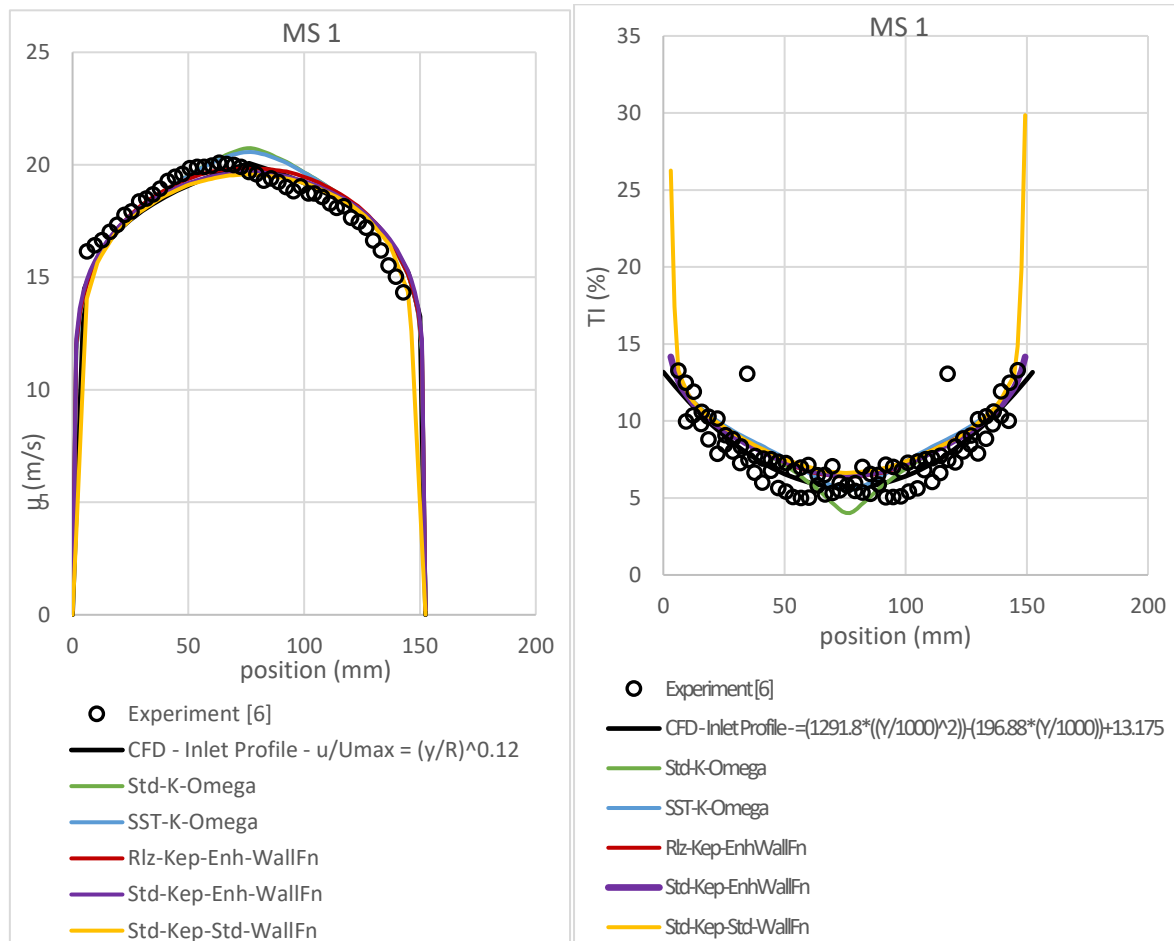

Figure 11. MS-1 - Velocity profile& TI profile – Effect of different Turbulence models

Station– MS-3

In station MS-3, represented in Figure 12, all the turbulence models used in the current simulations, perform very similar to one another when comparing the velocity profiles and TI profiles at the center of the channel. Both the k-ω models slightly over predict the velocity values towards the core wall, when compared to the other turbulence models used. The std k-ω also under predicted the velocity values toward the nacelle wall. These differences between the turbulence models in the velocity profiles were reflected in the TI profiles, resulting in std k-ω having a large difference in the TI profile towards the nacelle wall region.
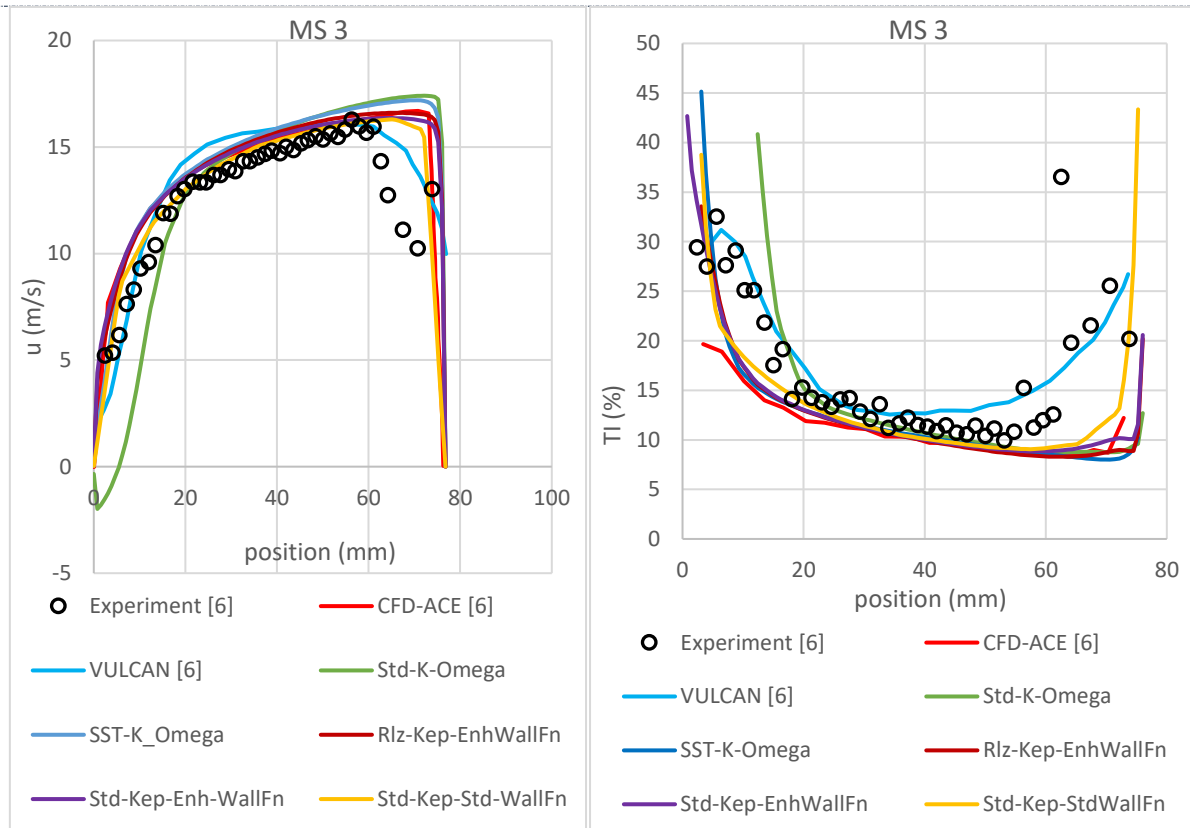
Figure 12. MS-3 - Velocity profile& TI profile – Effect of different Turbulence models

Station–MS-5

At station MS-5, results presented in figure 13, it is again both the k-ω models that show the largest difference between the various models used, with standard k-ω providing the poorest agreement. Both std k-ω and SST k-ω show a recirculation region at the nacelle wall near the exit of the inlet transition duct. Although SST k-ω only shows a very slight recirculation zone, about 5% of the channel height, whereas the recirculation zone is much larger in the simulation using std k-ω, with it being about 38% of the channel height. Overall std k-ω severely underpredicts the velocity values across most of the channel, while it severely over predicts just before reaching the core wall. SST k-ω also underpredicts velocity values near the nacelle wall while slightly over predicts as we approach the core wall. This might be due to the skewed nature of the structured mesh at the transition zone, but a very fine mesh of about 6 million elements was used to reduce the degree of skewness, thereby negating any effect the skewness might have on the computations. But then again, the other turbulence models (std k-ε with enhanced wall functions and the realizable k-ε with enhanced wall functions) both used the same mesh as the k-ω models without experiencing the same issues, indicating that it is most likely not an effect of the mesh. When comparing the TI profiles, the std k-ε models perform the best, having a good agreement with CFD-ACE computations, albeit exhibiting a large difference with the experimental values near the nacelle wall. Realizable k-ε produced slightly poorer results than the std k-ε models, by over predicting the TI values by 15% when compared to the std k-ε models. However, the SST k-ω greatly over predicted the TI by approximately 48% when compared to the std k-ε model, while the Std k-ω was the poorest, where, the effect of the large recirculation zone was clearly reflected in the TI values.
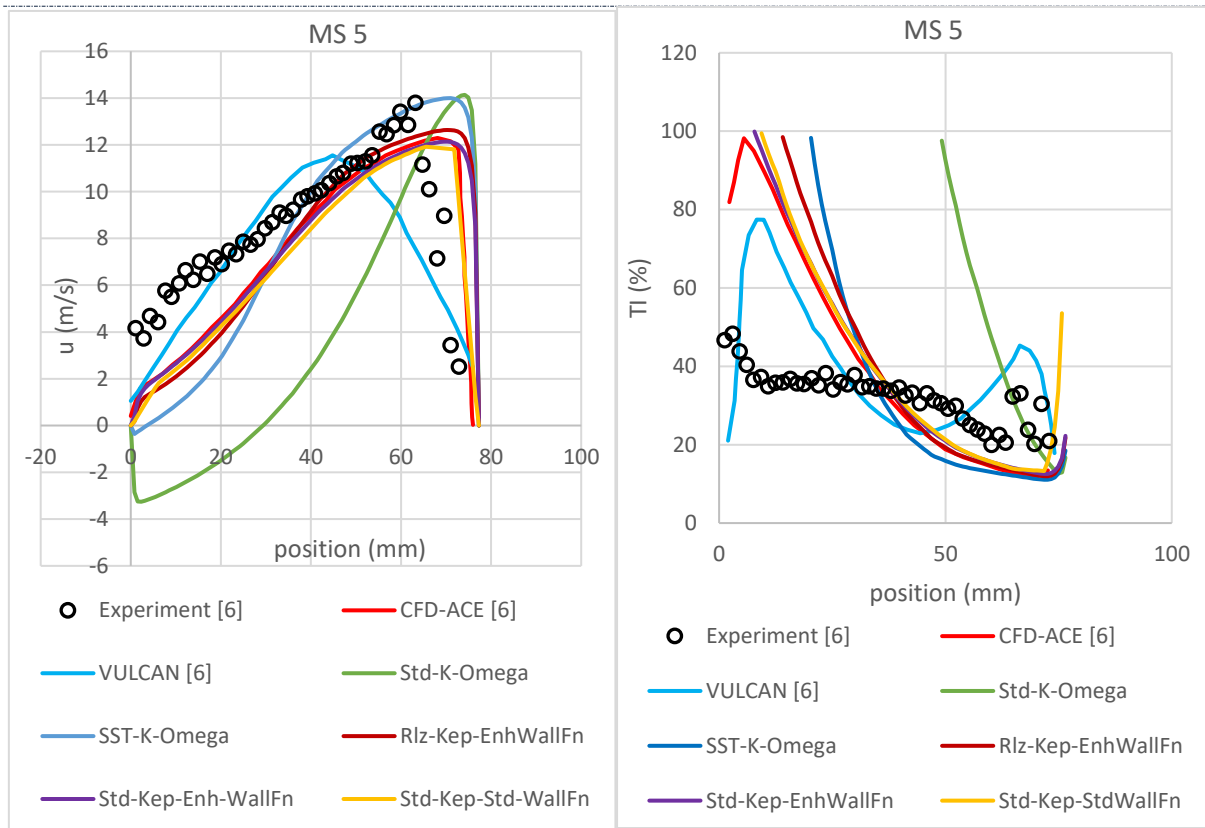
Figure 13. MS-5 - Velocity profile & TI profile – Effect of different Turbulence models

Station –MS-7

At station MS-7, the effects felt in the previous station seem to have carried forward,with both k-ω models showing considerable difference when compared to the other turbulence models used, as shown in figure 14. The SST k-ω underpredicts velocity near the nacelle wall when compared with experimental values, with an increasing trend across the channel to the point where it over predicts velocity values near the core wall. This is reflected in the TI profiles with higher TI presented near the nacelle walls and lower TI near the core walls. The std k-ω on the other hand severely under predicts the velocity values, roughly being 75% off the experimental values. This is again reflected in the TI profile with the std k-ω ending up over predicting the TI values. The std k-ε models perform very similar to one another, with both showing very good comparison with the CFD-ACE data and an excellent comparison with the experimental mean velocity data. They both under predict the TI values, but again show a very good comparison with the CFD-ACE data. The realizable k-ε models slightly under predicts the TI values when compared to the std k-ε models but still performs better than the VULCAN model.
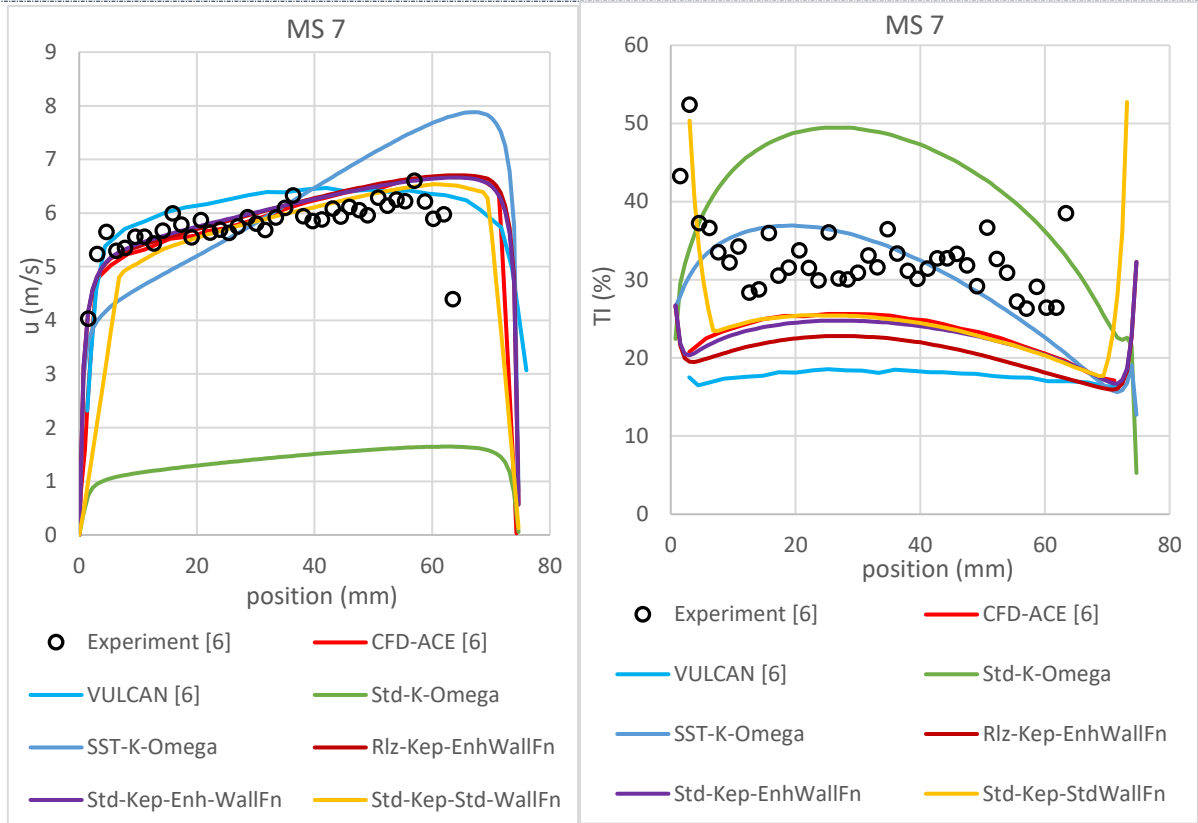
Figure 14. MS-7 - Velocity profile& TI profile – Effect of different Turbulence models

Station –MS-9

At station MS-9, most of the differences between the turbulence models seemed to have died out, except for the std k-ω turbulence model as shown in figure 15. The severely underpredicted velocity values by std k-ω seemingly carried over from the previous station, causing to under predict the velocity values in the current station as well although with a slightly improved comparison, with an average difference of about 36% when compared with the experimental values. This is reflected in the TI values where the std k-ω predicts higher values of TI when compared to the other turbulence models, which results in a surprisingly good comparison with the experimental values. In terms of the velocity comparisons, all other turbulence models studied showed a good comparison with one another were in excellent agreement with both the experimental values as well as the CFD-ACE data. In terms of TI comparison the std k-ε models performed very similarly to one another with an excellent agreement with CFD-ACE data, while the SST k-ω predicted slightly higher TI values which resulted in better comparison with the experimental values while the realizable k-ε predicted slightly lower TI values resulting in poorer comparison with the experimental data.
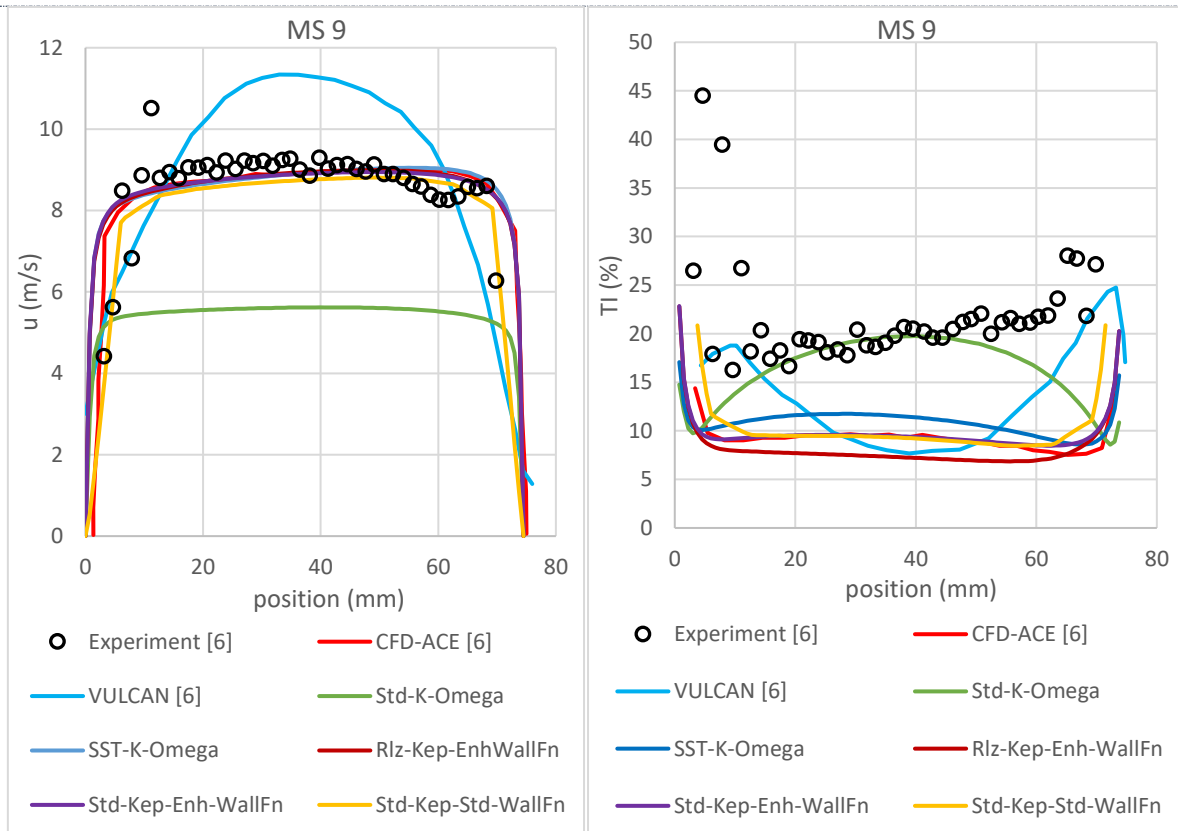
Figure 15. MS-9 - Velocity profile & TI profile – Effect of different Turbulence models

Station –MS-11
At station MS-11, all models predict approximately the same mean velocity levels, with the SST k-ω, realizable k-ε & std k-ε with enhanced wall functions, being able to capture a small wake region. The std k-ω again shows the poorest comparison with it predicting slightly lower mean velocity values with an asymmetric profile. This carries on in the TI comparisons, with all models showing similar TI profiles, severely underpredicting the TI values when compared to the experimental values, but again the reference study [6] attributed the high TI values to possible noise in the measurements. The comparisons can be seen in figure 16.
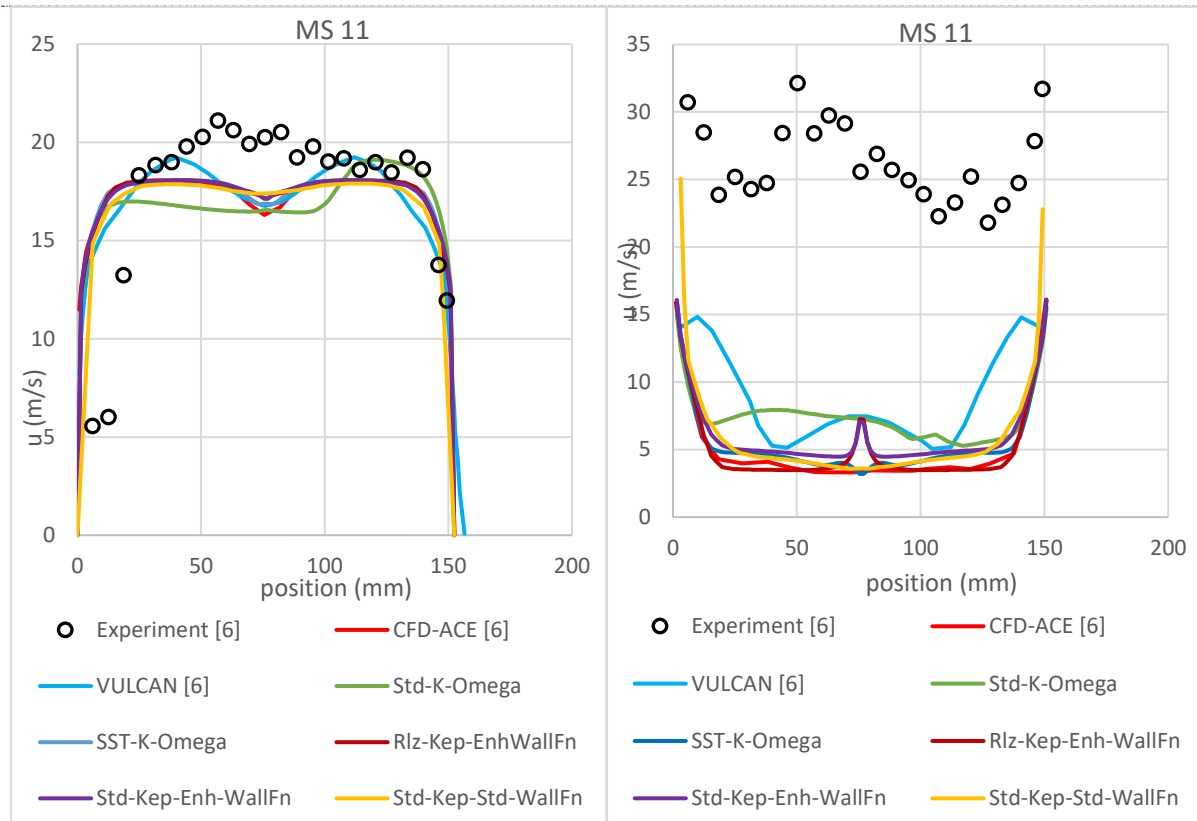
Figure 16. MS-11 – Velocity profile & TI profile – Effect of different Turbulence models

From the above plots, it could be seen that though most of the turbulence models considered showed better resolution at the walls, they were not able to overcome the differences at the regions noted earlier. Furthermore, the standard k-ω model performed poorly, underpredicting velocity values in many regions. Also, the std k- ω presented an asymmetric profile at station MS11. The realizable and the standard k-ε models using the enhanced wall functions were able to capture the wake region. But overall none of the turbulence models considered showed any considerable improvement when compared to the standard k-ε turbulence model employing standard wall function. From this work it can be inferred that the standard k-ε turbulence model with standard wall functions should be sufficient for use in the next phase of simulations where clutter will be incorporated into the nacelle.

4. SUMMARY
The study of airflow in a generic uncluttered nacelle was conducted as an important first step in setting up the basis for further analysis of suppressant transport within an aircraft engine nacelle. This initial study helped establish a viable CFD model to study the nacelle air flow conditions by studying the effects of different turbulence models, boundary conditions as well as the computational grids used in the simulation. Validation cases were run based on the experiments and CFD done by SNL using different input conditions and established multiple methods of running the computational models. The effects of computational grids were studied by carrying out a grid sensitivity study and it was concluded that Delaunay meshes provided the best results. The sensitivity of the simulations to different turbulence models, was also studied, to see if the discrepancies in the velocity and turbulence intensity profiles, near the walls, noticed in some sections, could be resolved. It was seen that none of the near- wall models provided an improved comparison and it was concluded that standard k-epsilon with standard wall functions gave the best results for the least computational expense. The standard k-ε employing enhanced wall functions was found to be a good option to get a good resolution near the walls, thereby making it an excellent option for when wall bounded clutter is to be added to the nacelle.

This provided a strong basis to continue and model suppressant injection and the effect of clutter elements. With a better understanding of the turbulence of the incoming airflow, guidance in the placement of the fire suppressant nozzles can be reliably provided.

5. NOMENCLATURE

ρ	Density	kg/m^3
$\bar{u}$	Mean component of velocity	m/s
u', v', w'	Fluctuating component of velocity	m/s
t	time	s
F	Body force per unit volume	N/m^3
p	Pressure	M/m^2
x, y, z	Position vector	m
μ	Dynamic viscosity	N s/m^2
TI	Turbulence Intensity	
u, v, w	Instantaneous velocity component	m/s
τ	Total shear stress	N/m^2
k	Turbulence kinetic energy	m^2/s^2
ε	Turbulence dissipation rate	m^2/s^3
ω	Specific dissipation rate	1/s
ν	Kinematic viscosity	m^2/s
β	Coefficient of thermal expansion	
P_k	Turbulence Production term	
P_b	Buoyancy Term	
i j	Tensor index	
LE	Leading Edge	
TE	Trailing Edge	
Y+	Non – dimensional wall distance	
$C_\mu, C_{1\epsilon}, C_{2\epsilon}, C_{3\epsilon}, \sigma_k \& \sigma_\epsilon$	Turbulence model constants	

REFERENCES

[1] R. G. Gann, "PROGRESS UNDER THE NEXT-GENERATION FIRE SUPPRESSION TECHNOLOGY PROGRAM (NGP) IN 1999," in Halon options technical working conference, 2000.

[2] A. Hamins, T. G. Cleary and J. Yang, "An analysis of the Wright Patterson full-scale engine nacelle fire suppression experiments," U.S. Dept. of Commerce, Technology Administration, National Institute of Standards and Technology, Gaithersburg, MD, 1997.

[3] B. Crawford, J. K. Watterson, S. Raghunathan and J. Warnock, "Modelling the dispersion of a fire suppressant through an idealised nacelle," in 44th AIAA Aerospace Sciences Meeting and Exhibit, Reno, NV, 2006.

[4] J. Hewson, S. Tieszen, W. Sundberg and P. DesJardin, "CFD modeling of fire suppression andits role in optimizing suppressant distribution," NIST Special Publication (NIST SP) - 984-4, 2003.

[5] J. C. Hewson and D. R. Keyser, "Predicting fire suppression in a simulated engine nacelle," NIST Special Publication (NIST SP) - 984-4, 2004.

[6] A. R. Black, J. M. Suo-Antilla, L. A. Gritzo, P. J. Disimile and J. R. Tucker, "Numerical Predictions and Experimental Results of Air Flow in a smooth Quarter-Scale Nacelle," Sandia National Laboratories Report, 2002.